Exosomes From ADSCs Attenuate Bleomycin-Induced Skin Fibrosis And Oxidative Stress In Scleroderma Via Circ-Zfyve9 Delivery

Zhidong Zhu
Fudan University
Hui Tang
Fudan University
Yiqi Zhu
Fudan University
Hao Wang (wh91351@126.com)
Shanghai Medical University: Fudan University
Yanyun Shen
Fudan University

Research

Keywords: adipose-derived stem cells (ADSCs), systemic sclerosis, exosome, oxidative stress, fibrosis, circ-Zfyve9

Posted Date: June 9th, 2021

DOI: https://doi.org/10.21203/rs.3.rs-551751/v1

Abstract

Background: Systemic sclerosis (SSc) is autoimmune trait affecting several organs, which is identified by thickening of dermis and connective tissue affected by collagen accumulation, as well as vascular injuries inducing hypoxia.

Methods: In this investigation, adipose-derived stem cells (ADSCs) were separated from the ADSC exosomes and a bleomycin-induced SSc mouse model was constructed. We employed high-throughput sequencing to study abnormal expression of circular RNAs (circRNAs) in SSc skin tissues with or without ADSC exosome treatment. The regulatory mechanism and targets were studied using bioinformatics analysis, luciferase reporting analysis, angiogenic differentiation experiments, and RT-qPCR detection.

Results: ADSC exosome treatment prevented dermal thickening and fibrosis in bleomycin-induced scleroderma. In addition, circ-Zfyve9 was demonstrated to have an important function in ADSC exosome-mediated skin tissue protection. GPX4 and miR-135 were shown to be circ-Zfyve9 downstream targets. Overexpressing miR-135 or downregulating GPX4 reversed circ-Zfyve9 promotion effects rupon angiopoiesis by promoting lipidosome ROS in EPCs under hypoxic conditions. Overexpressing miR-135 or downregulating GPX4 reversed the circ-Zfyve9 inhibition effect on fibrosis in myofibroblasts under hypoxic conditions. Overexpressing circ-Zfyve9 increased the therapeutic effect of ADSC exosomes.

Conclusions: Taken together, the present study results show that the exosomes from ADSCs attenuate bleomycin-induced skin fibrosis and oxidative stress in scleroderma via circ-Zfyve9 delivery.

Introduction

Systemic sclerosis (SSc) is well recognized as scleroderma, which is an autoimmune connective tissue disorder identified by adaptive and innate immunity dysregulation, microvascular damage, and generalized skin fibrosis, as well as multiple organs [1]. Skin fibrosis is thus an important SSc symptom. Pathological alterations in organs including heart, kidneys, lungs and gastrointestinal tract, determine possibility of clinical improvements. Ten-year survival was 55% in a diffuse cutaneous disorder cohort [2]. Fibrosis usually affects the mouth and face, leading to skin tightening, lip retraction, and irreversible scarring. The oral aperture that narrowed influences speech, dental structure, psychological status and facial expression together with life quality [3].

Former investigations have illustrated that mesenchymal stem cells (MSCs) serve as the therapy target to halt SSc progression [4]. It is inferred that adipose-derived stem cell (ADSC) transplantation can mitigate SSc-related fibrosis pathogenesis [5–7]. Several studies have confirmed the therapeutic effect of ADSC exosomes on SSc via exosome delivery. Exosomes are small (~ 30–100 nm) membrane vesicles that are released from disparate classes of cells in response to specific cellular stimulation [8]. They have a crucial messenger function in intercellular communication of delivering pre-wrapped cargoes, like miRNAs, circRNA, and proteins, to recipient cells [9]. Previous studies have found that ADSC-derived exosomes (ADSC-Exos) are internalized in fibroblasts and help cutaneous wound healing via promoting

cell proliferation, collagen synthesis, and migration [10]. The ADSC exosome roles in SSc remain unknown. The present investigation aimed to reveal the regulatory role and mechanism of ADSC exosomes in SSc.

Materials And Methods

Reagents & cells

We obtained adipogenic differentiation medium, osteogenic differentiation medium, Dulbecco's Modified Eagle's medium (DMEM), and fetal bovine serum (FBS) from Nego (Shanghai, China). Antibodies against CD31, CD29, CD44, CD104, CD90, Von Willebrand factor (vWF), GAPDH, and fluorescein isothiocyanate were purchased from Sigma-Aldrich (St. Louis, MO, USA). We obtained myofibroblasts and EPCs from Procell Life Science Co., Ltd. (Wuhan, China).

Animals and ethics statement

Animal Care and Utilization Committee at Huashan hospital of Fudan University supervised all animal procedures. Our lab purchased male C57BL/6 mice with four-week age from SLAC Laboratory Animal Co. Ltd (Shanghai, China). We housed animals individually and independently in ventilated cages at 24–26°C and constant humidity in a 12-h light/dark cycle environment. Ethics Committee in Huashan Hospital of Fudan University oversaw all experiments. All surgical procedures were performed under anesthesia with an intraperitoneal injection of 30 mg/kg sodium pentobarbital.

ADSC culture, isolation, and identification

Technician washed harvested adipose tissue samples from healthy subjects (consent was obtained from patients via a volunteer) or normal rats with phosphate-buffered saline (PBS), minced in 0.2% collagenase I (Sigma-Aldrich, St. Louis, MO, USA), and digested for one hour at 37°C with intermittent shaking. The samples were then cleaned and further digested in DMEM (Sigma-Aldrich, St. Louis, MO, USA) containing 15% FBS (Gibco BRL, Frederick, MD, USA). The tissues samples were centrifuged at 1000 rpm for ten minutes to erase mature adipocytes. Tissue pellets were subsequently resuspended in DMEM supplied with FBS of 15%, 100 μg/mL streptomycin, and 100 U/mL penicillin, which were cultured at 37°C with 5% CO_2. We treated ADSCs at ~80–90% confluency with 0.02% ethylenediaminetetraacetic acid/0.25% trypsin (Sigma-Aldrich, St. Louis, MO, USA) for five minutes under room temperature, which were then replated. Fluorescein isothiocyanate-conjugated CD90, CD29, CD105, vWF, and CD44 antibodies were used for phenotypic analysis. IgG-matched isotype was used as an internal control for every antibody. Our lab cultured normoxic ADSCs in 95% air (O_2 of 20%) and CO_2 of 5% .

Multilineage ADSC differentiation

To validate ADSC multilineage differentiation, third-passage mouse ADSCs were cultured in adipogenic differentiation medium (Sigma-Aldrich, St. Louis, MO, USA). They were then stained leveraging Oil Red O

in two weeks or cultured in osteogenic differentiation medium (Sigma-Aldrich, St. Louis, MO, USA), which were stained utilizing Alizarin Red after three weeks.

ADSC-Exo identification and isolation

After getting ~80–90% confluency, we rinsed ADSCs with PBS and then cultured them in FBS-free endothelial cell growth medium-2MV supplied using 1 × serum replacement solution (PeproTech, NJ, USA) for two more days. We collected and centrifuged culture medium at 300 *g* for ten minutes and then at 2000 *g* for ten minutes to erase cellular debris and apoptotic cells. After centrifugation at 10,000 *g* for 0.5 h, we filtered supernatant using 0.22-μm filter (Millipore, Billerica, USA). Then, 15 mL of the supernatant were transferred to Amicon Ultra-15 Centrifugal Filter Unit (100 kDa; Millipore), which were centrifuged at 4000 *g* to achieve a volume of ~1 mL. Our team cleaned ultrafiltration unit using PBS twice, which was centrifuged at 4000 *g* to achieve 1 mL volume. We resuspended exosome pellets in 500 μL PBS at 4ºC. Exosome protein content was detected employing the Pierce bicinchoninic acid (BCA) Protein Assay Kit (Thermo Fisher Scientific, MA, USA). We maintained exosomes at -80°C until further use. We applied western blotting (WB) and transmission electron microscopy to characterize exosomes. We determined size using dynamic light scattering with Nanosizer (Malvern Instruments, Malvern, UK). Size distribution with particle radius (nm) were represented on the x-axis and percentage on the y-axis.

Model treatment and establishment

We generated bleomycin-induced murine fibrosis model following a previous protocol [4]. Then, 100 μL bleomycin (1 mg/mL) were subcutaneously injected into shaved area on mouse's back (1 cm^2) with 27-gauge needle. Our lab carried out injections daily for three consecutive weeks. Mice in control group received 100 μl of PBS.

For treatments, we randomly divided bleomycin-induced SSc mice into PBS (controls), Exo, circ-Zfyve9-Exo, mimic+circ-Zfyve9-Exo, and si-GPX4+circ-Zfyve9-Exo groups. We subcutaneously injected animals in each group with 100 μL PBS having or not BMSCs (1×10^6) 22 d after bleomycin induction. We sacrificed mice 3, 7, and 14 d after first injection. Skin tissue samples within shaved area were then collected for further study. There were ≥6 mice in every group.

Strand-specific RNA-Seq library and RNA-Seq

Our team extracted total RNA from skin tissue with or without exosome treatment applying TRIzol Reagent (Invitrogen, Carlsbad, CA, USA). We processed ~3 μg total RNA from every sample using VAHTS Total RNA-Seq (H/M/R) Library Prep Kit (Illumina; Vazyme Biotech Co., Ltd, Nanjing, China) to eliminate ribosomal RNA preserving other RNA, such as mRNA. RNA samples were dealt with RNase R (Epicenter, 40 U, 37°C for 3 h) and purified by TRIzol. The RNA-Seq library was made utilizing KAPA Stranded RNA-Seq Library Prep Kit (Roche, Basel, Switzerland), which were subjected to deep sequencing via Illumina HiSeq 4000.

Quantitative real-time polymerase chain reaction (qPCR)

Our team extracted total RNA from cells employing a TRIzol reagent kit (Invitrogen, Carlsbad, CA, USA) following standard protocol. Then, we synthesized and amplified cDNA employing a TaqMan miRNA reverse transcription kit. Primers used to assay circ-Zfyve9 expression were as follows: forward, 5'-GGCATCACTGCAGAGCG-3' and reverse, 5'-CTTATTCCACTTTGTATCC-3'. GPX4 primers were as follows: forward, 5'-TGTGCATCCCGCGATGATT-3' and reverse, 5'-CCCTGTACTTATCCAGGCAGA-3'. GAPDH primers were as follows: forward, 5'-AGGTCGGTGTGAACGGATTTG-3' and reverse, 5'-GGGGTCGTTGATGGCAACA-3'. Finally, miR-135 primers were as follows: forward, 5'-GAAATGGTTTTGAAGTCG-3' and reverse, 5'-CGTTCCAGAGGCTCTAGTT-3'. Then, qPCR was conducted using a TaqMan human miRNA assay kit. We used $2^{-\Delta\Delta CT}$ method to calculate relative expression fold changes. *U6* and *GAPDH* were used as internal references.

Luciferase reporter assay

We amplified entire GPX4 and circ-Zfyve93'-UTR fragment containing miR-135 binding sites, which were inserted into downstream firefly luciferase reporter gene in pmirGLO plasmid (Promega Corp., Madison, WI, USA). GPX4 and circ-Zfyve9 sequences interacting with the miR-135 seed region were mutated using site-directed gene mutagenesis kit (Beyotime Institute of Biotechnology, Beijing, China). They were then cloned into the luciferase reporter plasmid. We named luciferase reporter plasmids that constructed pmirGLO-GPX4-3'-UTR-WT, pmirGLO-circ-Zfyve9-WT, pmirGLO-GPX4-3'-UTR-MUT, and pmirGLO-circ-Zfyve9-MUT. For the luciferase reporter assay, we co-transfected 293T cells using 10 ng pmirGLO control vectors, 20 ng of constructed luciferase reporter plasmids, and 25 nM miR-NC or miR-135 using Lipofectamine 2000 (Invitrogen). Luciferase function was detected utilizing dual luciferase reporter system (Promega) two days post-transfection. We applied Renilla luciferase activity for normalization.

Tubule formation assay

In vitro neovascularization was assayed in human fibrin matrices. Following treatment, serum-starved EPCs in endothelial basal medium were seeded onto six-well plates coated with Matrigel (10^5 cells/well; BD Biosciences, Franklin Lakes, NJ, USA), which were incubated at 37°C for 0.5 d. Tubular structures that formed in the Matrigel were observed and photographed using phase-contrast microscopy. The newly formed tube lengths in ten randomly selected fields per well were measured.

WB assay

We centrifuged cell and tissue lysates at 12,000 rpm at 4°C following protease inhibitor addition. Protein concentration was captured using Pierce BCA kit (Thermo Fisher). We separated proteins using 10% SDS-PAGE, which were transferred to PVDF membranes. Primary antibodies for CD63 (1:600), CD81 (1:600), TGF-β (1:1000), α-SMA (1:1000), collagen I (1:500), and anti-GAPDH (1:1000, Sigma-Aldrich) were used to assay protein expression. Horseradish peroxidase-conjugated secondary antibody (1:1000, Abcam, USA). Our lab utilized ECL kit (Millipore, Burlington, MA, USA) to obtain bands.

Histological examination

We fixed skin tissue samples in each group in 10% formalin solution, which we embedded in paraffin. We stained thin 5-μm sections using Masson's trichrome, followed by CD31 staining to establish histopathological angiogenesis alternations. Our team tested sections utilizing Axiophot light microscope (Zeiss, Oberkochen, Germany) or ECLIPSE E600 fluorescence microscope (Nikon, Tokyo, Japan), which were photographed.

ROS production analysis

Our lab measured ROS production in skin scar tissue samples using 2',7'-dichlorofluorescin diacetate (Molecular Probes, Eugene, OR, USA). Lipidosome ROS production in cells was detected using a C11 BODIPY581/591 Lipid Peroxidation Sensor (MKBio, Shanghai, China).

Statistical analysis

Results were expressed as means ± standard deviation (SD). GraphPad Prism (GraphPad, La Jolla, CA, USA) was leveraged to analyze differences among groups. P-values ≤ 0.05 were regarded as statistical significance.

Results

Characterization of ADSC-Exo

Our previous study demonstrated that exosomes have an important function in MSC-mediated wound healing [11]. In order to confirm whether exosomes from ADSCs function in bleomycin-induced skin fibrosis and oxidative stress. ADSCs isolated from mouse adipose tissue had classic cobblestone-like morphology (Figure 1A). Immunofluorescence data demonstrated that ADSCs expressed cell surface markers CD44, CD105, CD29 and CD90, while not endothelial marker vWF (Figure 1B–G). Oil Red O along with Alizarin Red staining results showed that ADSCs have a differentiation potential after induction of osteoblast and adipocyte differentiation (Figure 1H–I).

Transmission electron microscopy illustrated that ADSC exosomes had ~100 nm size (Figure 1J). Nanosizer analysis of exosome particle size also showed that exosomes isolated from ADSCs were ~100 nm in size (Figure 1K). WB detection showed that ADSC exosomes expressed CD81 and CD63 (Figure 1L), suggesting that nanoparticles were actually exosomes.

ADSC exosome treatment prevents dermal thickening and fibrosis in bleomycin-induced scleroderma

Masson's trichrome staining results in bleomycin-induced murine fibrosis model showed that collagen deposition was increased in bleomycin-induced scleroderma, while ADSC exosome treatment significantly decreased collagen deposition (Figure 2A and B). Immunofluorescence detection of ROS staining validated that ADSC exosome treatment decremented ROS accumulation significantly in

bleomycin-induced scleroderma (Figure 2C and D). Immunohistochemical CD31 staining showed that angiogenesis was decreased in bleomycin-induced scleroderma. ADSC exosome treatment significantly reversed the inhibitory effect of scleroderma on angiogenesis (Figure 2E and F). WB for fibroblast-associated proteins TGF-β, collagen I, and α-SMA showed that ADSC exosome treatment significantly decreased collagen I, α-SMA, and TGF-β expression in bleomycin-induced scleroderma (Figure 2G–J).

circ-Zfyve9 has an important function in ADSC exosome-mediated skin tissue protection

Several studies have found that circRNA has an important function in organizational microenvironment regulation [12]. In order to determine whether ADSC exosome-mediated skin tissue protection via circRNA delivery. Our team utilized high-throughput sequencing to detect abnormal circRNA expression in scleroderma skin, with or without ADSC exosome treatment. Heatmap analysis demonstrated that ADSC exosome treatment resulted in different circRNA expression levels (Figure 3A). A total of 574 upregulated and 1707 downregulated circRNAs were found in ADSC exosome-treated scleroderma skin when compared to scleroderma skin without treatment (Figure 3B). RT-qPCR showed that seven circRNAs from the sequencing analyses were upregulated, including mmu_circ_0000376, mmu_circ_0001240, mmu_circ_0002870, mmu_circ_0009688, mmu_circ_0011768, and mmu_circ_0011922. Data illustrated that only the mmu_circ_0001240 expression was upregulated in ADSC exosome-treated scleroderma skin when compared to scleroderma skin without treatment (Figure 3C). Bioinformatics analysis found that mmu_circ_0001240 originated from the *Zfyve9* gene exon (2024 bp) and was located in chr4:108390393-108392417. The mmu_circ_0001240 was named circ-Zfyve9 (Figure 3D).

GPX4 and miR-135 are circ-Zfyve9 downstream targets

Bioinformatics results verified that circ-Zfyve9 can interact with a bunch of miRNAs, including miR-493-3p, miR-193, miR-431, miR-135, miR-770, miR-1960, and miR-760. A luciferase reporter vector with circ-Zfyve9 sequence was then constructed and transfected into HEK293 cells using different miRNA mimics. The results showed that miR-135 can decreament significantly fluorescein intensity, suggesting that miR-135 is circ-Zfyve9 downstream target (Figure 4A). Luciferase reporter analysis verified that miR-135 inhibited luciferase activity in wild-type (WT), but not in mutated (MUT) cell lines (Figure 4B and C), saying that miR-135 is a circ-Zfyve9 target.

Bioinformatics results demonstrated that GPX4 is miR-135 downstream target. To further show a correlation between GPX4 and miR-135, we incorporated WT or MUT 3'UTR-GPX4 sequences including an miR-135 binding sequence into luciferase reporter vector (Figure 4D). Our team transfected luciferase reporter vector into HEK293 cells, with or not miR-135 mimic. Luciferase reporter analysis showed that miR-135 inhibited luciferase function in WT, yet not in MUT cell lines (Figure 4E), verifying that GPX4 is an miR-135 target.

RT-qPCR results illustrated that circ-Zfyve9 expression was enriched in both EPCs and myofibroblasts after transfection using circ-Zfyve9 overexpression vector. Treatment with an miR-135 mimic or GPX4 silencing had no effect on circ-Zfyve9 expression in EPCs and myofibroblasts (Figure 4F and G),

suggesting that both miR-135 and GPX4 are located downstream of circ-Zfyve9. RT-qPCR detection also found that circ-Zfyve9 overexpression decreased miR-135 expression. GPX4 silencing had no effect on circ-Zfyve9-induced miR-135 inhibition (Figure 4H and I), suggesting that miR-135 is located between circ-Zfyve9 and GPX4. The results also found that circ-Zfyve9 overexpression increased GPX4 expression, while miR-135 upregulation reversed the promotion effect of circ-Zfyve9 on GPX4 expression. GPX4 expression decremented significantly after transfection with a GPX4 silencing vector (Figure 4J and K), advising that circ-Zfyve9 enhanced GPX4 expression through sponging miR-135.

miR-135 overexpression or GPX42 downregulation reversed the promotion of circ-Zfyve9 on angiopoiesis in EPCs under hypoxic conditions

EPC tube formation capability evaluations showed that circ-Zfyve9 overexpression promoted angiogenic differentiation of EPCs under hypoxic conditions. Overexpression of miR-135 or GPX4 silencing reversed the promotion of circ-Zfyve9 on the angiogenic differentiation of EPCs under hypoxic conditions (Figure 5A and B), suggesting that miR-135 overexpression or GPX42 downregulation reversed circ-Zfyve9 promotion on angiopoiesis in EPCs under hypoxic conditions. Immunofluorescence detection showed that circ-Zfyve9 overexpression decreased liposomal oxidative stress by decreasing oxidized liposomes. Overexpression of miR-135 or GPX4 silencing reversed inhibitory circ-Zfyve9 effect upon hypoxia-induced liposome oxidative stress (Figure 5C and D).

Overexpression of miR-135 or GPX4 downregulation reversed the circ-Zfyve9 inhibitory effect on fibrosis in myofibroblasts under hypoxic conditions

WB detection showed that circ-Zfyve9 overexpression decreased fibroblast-associated protein TGF-β, collagen I, and α-SMA expression in myofibroblasts under hypoxic conditions. Overexpression of miR-135 or GPX4 silencing reversed circ-Zfyve9 inhibitory effect upon hypoxia-induced fibroblast-associated protein TGF-β, collagen I, and α-SMA expression (Figure 6A–D).

Overexpressing circ-Zfyve9 increased the therapeutic effect of ADSC exosomes

Immunohistochemical detection of apoptotic skin tissues showed the ADSC exosomes after treatment with overexpressed circ-Zfyve9. Apoptosis in skin tissues of bleomycin-induced scleroderma was decreased when compared to the ADSC exosome treatment group. Overexpression of miR-135 or GPX4 silencing reversed the protective effect of circ-Zfyve9 exosomes on apoptosis inhibition in bleomycin-induced scleroderma skin (Figure 6A and B), suggesting that circ-Zfyve9 overexpression increased the therapeutic effect of ADSC exosomes.

Discussion

Several studies have found that ADSC transplantation therapy can reverse scleroderma-induced cutaneous fibrosis [13, 14]. Exosome secretion by ADSCs plays an important role in microenvironmental regulation via delivery of bioinformatics molecule [15, 16]. The present study found that ADSC exosome

treatment avoids dermal thickening and fibrosis induced by bleomycin administration. In addition, ADSC exosome treatment inhibited scleroderma-induced ROS and reversed the inhibitory effect on angiogenesis in scleroderma, suggesting that ADSC exosomes have a therapeutic effect in scleroderma.

Accumulating studies have reported that circRNA has an important function in the regulation of the stress microenvironment [17]. Whether circRNA has an indispensable regulatory role in scleroderma remains unclear. High-throughput sequencing found that the ADSC exosome treatment group had an abnormal expression of circRNA compared to the scleroderma group. RT-qPCR analysis showed that mmu_circ_0001240 has an important function in ADSC exosome-mediated skin tissue protection. Mmu_circ_0001240 originates from *Zfyve9* gene exon (2024 bp) and is located in chr4:108390393–108392417. It was named circ-Zfyve9. It has also been confirmed that circRNA can regulate gene expression by sponging miRNA [18, 19]. The current investigation discovered that circ-Zfyve9 can interact with many miRNAs including miR-493-3p, miR-193, miR-431, miR-135, miR-770, miR-1960, and miR-760. Luciferase reporter assay confirmed that only miR-135 has more conserved binding sites. RT-qPCR detection verified that circ-Zfyve overexpression inhibits miR-135 expression. miR-135 overexpression reversed protective circ-Zfyve effect upon angiopoiesis in EPCs under hypoxic conditions, while miR-135 upregulation reversed the inhibitory circ-Zfyve effect upon hypoxia-induced fibrosis in myofibroblasts.

Luciferase reporter analysis discovered that miR-135 can interact with GPX4. GPX4 catalyzes lipid peroxide reduction in complex cellular membrane environment [20]. Lipid peroxidation has been reported in knockout models, strengthening the GPX4 to protect cells from detrimental lipid peroxide effects [21, 22]. In this study, circ-Zfyve overexpression promoted GPX4 expression. Overexpression of miR-135 or GPX4 silencing reversed circ-Zfyve protective effect upon angiopoiesis in EPCs under hypoxic conditions. Overexpression of miR-135 or GPX4 silencing also reversed circ-Zfyve inhibitory effect upon hypoxia-induced fibrosis in myofibroblasts. Immunofluorescence detection showed that circ-Zfyve9 overexpression decreased liposomal oxidative stress by decreasing oxidized liposomes. However, miR-135 overexpression or GPX4 silencing reversed circ-Zfyve9 inhibitory effect upon hypoxia-induced liposome oxidative stress. This suggests that GPX4 and miR-135 are downstream targets of circ-Zfyve9. Overexpressing circ-Zfyve9 increased the therapeutic effect of ADSC exosomes on scleroderma.

Conclusion

In conclusion, current investigation determined that ADSC exosomes attenuate bleomycin-induced skin fibrosis and oxidative stress in scleroderma via circ-Zfyve9 delivery.

Declarations

Acknowledgements

Not applicable.

Abbreviations

SSc, systemic sclerosis; ADSCs, adipose-derived stem cells; DMEM, Dulbecco's Modified Eagle's medium; circRNAs, circular RNAs; MSCs, mesenchymal stem cells; FBS, fetal bovine serum; vWF, Von Willebrand factor.

Authors' contributions

ZZ and YS wrote the manuscript. HT, YZ, and HW edited manuscript. All authors approved the final manuscript.

Funding

Shanghai Health and Family Planning Commission (20184Y0024).

Consent for publication

All figures and tables in this manuscript are original and all authors approved the submission.

Data and material availability

Not applicable.

Competing interests

None declared.

Ethics Approval and Consent to Participate

Animal Care and Utilization Committee at Huashan hospital of Fudan University supervised all animal procedures. Our lab purchased male C57BL/6 mice with four-week age from SLAC Laboratory Animal Co. Ltd (Shanghai, China). We housed animals individually and independently in ventilated cages at 24–26°C and constant humidity in a 12-h light/dark cycle environment. Ethics Committee in Huashan Hospital of Fudan University oversaw all experiments. All surgical procedures were performed under anesthesia with an intraperitoneal injection of 30 mg/kg sodium pentobarbital.

References

[1] Y. Allanore, O. Distler, Systemic sclerosis in 2014: Advances in cohort enrichment shape future of trial design, Nat Rev Rheumatol, 11 (2015) 72-74.

[2] V.D. Steen, T.A. Medsger, Jr., Severe organ involvement in systemic sclerosis with diffuse scleroderma, Arthritis Rheum, 43 (2000) 2437-2444.

[3] A. Del Rosso, S. Maddali-Bongi, Oral health in patients with systemic sclerosis, Rheumatology (Oxford), 53 (2014) 1355-1356.

[4] M. Jiang, Y. Yu, J. Luo, Q. Gao, L. Zhang, Q. Wang, J. Zhao, Bone Marrow-Derived Mesenchymal Stem Cells Expressing Thioredoxin 1 Attenuate Bleomycin-Induced Skin Fibrosis and Oxidative Stress in Scleroderma, J Invest Dermatol, 137 (2017) 1223-1233.

[5] C. Capelli, E. Zaccara, P. Cipriani, P. Di Benedetto, W. Maglione, R. Andracco, G. Di Luca, F. Pignataro, R. Giacomelli, M. Introna, C. Vitali, N. Del Papa, Phenotypical and Functional Characteristics of In Vitro-Expanded Adipose-Derived Mesenchymal Stromal Cells From Patients With Systematic Sclerosis, Cell Transplant, 26 (2017) 841-854.

[6] M. Griffin, C.M. Ryan, O. Pathan, D. Abraham, C.P. Denton, P.E. Butler, Characteristics of human adipose derived stem cells in scleroderma in comparison to sex and age matched normal controls: implications for regenerative medicine, Stem Cell Res Ther, 8 (2017) 23.

[7] I. Rosa, E. Romano, B.S. Fioretto, M. Matucci-Cerinic, M. Manetti, Adipose-derived stem cells: Pathophysiologic implications vs therapeutic potential in systemic sclerosis, World J Stem Cells, 13 (2021) 30-48.

[8] M. Tkach, C. Thery, Communication by Extracellular Vesicles: Where We Are and Where We Need to Go, Cell, 164 (2016) 1226-1232.

[9] A. Rustom, R. Saffrich, I. Markovic, P. Walther, H.H. Gerdes, Nanotubular highways for intercellular organelle transport, Science, 303 (2004) 1007-1010.

[10] L. Hu, J. Wang, X. Zhou, Z. Xiong, J. Zhao, R. Yu, F. Huang, H. Zhang, L. Chen, Exosomes derived from human adipose mensenchymal stem cells accelerates cutaneous wound healing via optimizing the characteristics of fibroblasts, Sci Rep, 6 (2016) 32993.

[11] W. Zhang, J. Zhu, X. He, X. Liu, J. Li, W. Li, P. Yang, J. Wang, K. Hu, X. Zhang, X. Li, H. Jing, Exosome complex genes mediate RNA degradation and predict survival in mantle cell lymphoma, Oncol Lett, 18 (2019) 5119-5128.

[12] Y. Wang, J. Liu, J. Ma, T. Sun, Q. Zhou, W. Wang, G. Wang, P. Wu, H. Wang, L. Jiang, W. Yuan, Z. Sun, L. Ming, Exosomal circRNAs: biogenesis, effect and application in human diseases, Mol Cancer, 18 (2019) 116.

[13] W. Chen, Z.K. Xia, M.H. Zhang, G.C. Ding, X.Y. Zhang, Z.X. Wang, R.Y. Yang, Adipose tissue-derived stem cells ameliorates dermal fibrosis in a mouse model of scleroderma, Asian Pac J Trop Med, 10 (2017) 52-56.

[14] J.J. Chia, T. Zhu, S. Chyou, D.C. Dasoveanu, C. Carballo, S. Tian, C.M. Magro, S. Rodeo, R.F. Spiera, N.H. Ruddle, T.E. McGraw, J.L. Browning, R. Lafyatis, J.K. Gordon, T.T. Lu, Dendritic cells maintain dermal adipose-derived stromal cells in skin fibrosis, J Clin Invest, 126 (2016) 4331-4345.

[15] J. Jin, Y. Shi, J. Gong, L. Zhao, Y. Li, Q. He, H. Huang, Exosome secreted from adipose-derived stem cells attenuates diabetic nephropathy by promoting autophagy flux and inhibiting apoptosis in podocyte, Stem Cell Res Ther, 10 (2019) 95.

[16] W. Gao, X. Wang, Y. Si, J. Pang, H. Liu, S. Li, Q. Ding, Y. Wang, Exosome Derived from ADSCs Attenuates Ultraviolet B-mediated Photoaging in Human Dermal Fibroblasts, Photochem Photobiol, (2020).

[17] J.G. Travers, F.A. Kamal, J. Robbins, K.E. Yutzey, B.C. Blaxall, Cardiac Fibrosis: The Fibroblast Awakens, Circ Res, 118 (2016) 1021-1040.

[18] M.L. Tornesello, R. Faraonio, L. Buonaguro, C. Annunziata, N. Starita, A. Cerasuolo, F. Pezzuto, A.L. Tornesello, F.M. Buonaguro, The Role of microRNAs, Long Non-coding RNAs, and Circular RNAs in Cervical Cancer, Front Oncol, 10 (2020) 150.

[19] A. Abi, N. Farahani, G. Molavi, S.M. Gheibi Hayat, Circular RNAs: epigenetic regulators in cancerous and noncancerous skin diseases, Cancer Gene Ther, 27 (2020) 280-293.

[20] R. Brigelius-Flohe, M. Maiorino, Glutathione peroxidases, Biochim Biophys Acta, 1830 (2013) 3289-3303.

[21] N. Yagoda, M. von Rechenberg, E. Zaganjor, A.J. Bauer, W.S. Yang, D.J. Fridman, A.J. Wolpaw, I. Smukste, J.M. Peltier, J.J. Boniface, R. Smith, S.L. Lessnick, S. Sahasrabudhe, B.R. Stockwell, RAS-RAF-MEK-dependent oxidative cell death involving voltage-dependent anion channels, Nature, 447 (2007) 864-868.

[22] W.S. Yang, R. SriRamaratnam, M.E. Welsch, K. Shimada, R. Skouta, V.S. Viswanathan, J.H. Cheah, P.A. Clemons, A.F. Shamji, C.B. Clish, L.M. Brown, A.W. Girotti, V.W. Cornish, S.L. Schreiber, B.R. Stockwell, Regulation of ferroptotic cancer cell death by GPX4, Cell, 156 (2014) 317-331.

Figures

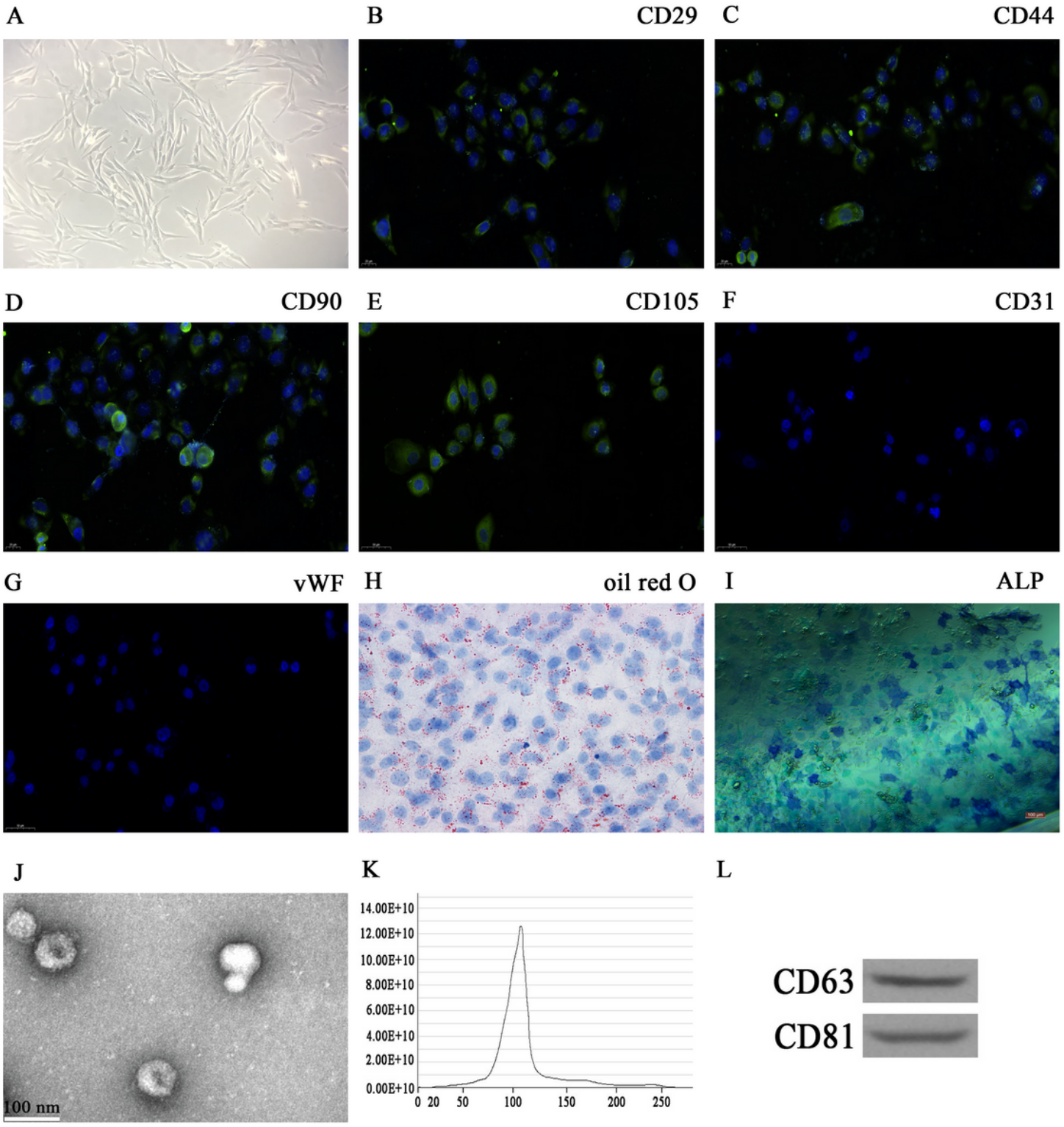

Figure 1

ADSCs isolated from mouse adipose tissue had classic cobblestone-like morphology (A). Immunofluorescence data demonstrated that ADSCs expressed cell surface markers CD44, CD105, CD29 and CD90, while not endothelial marker vWF (B–G). Oil Red O along with Alizarin Red staining results showed that ADSCs have a differentiation potential after induction of osteoblast and adipocyte differentiation (H–I). Transmission electron microscopy illustrated that ADSC exosomes had ~100 nm

size (J). Nanosizer analysis of exosome particle size also showed that exosomes isolated from ADSCs were ~100 nm in size (K). WB detection showed that ADSC exosomes expressed CD81 and CD63 (L), suggesting that nanoparticles were actually exosomes.

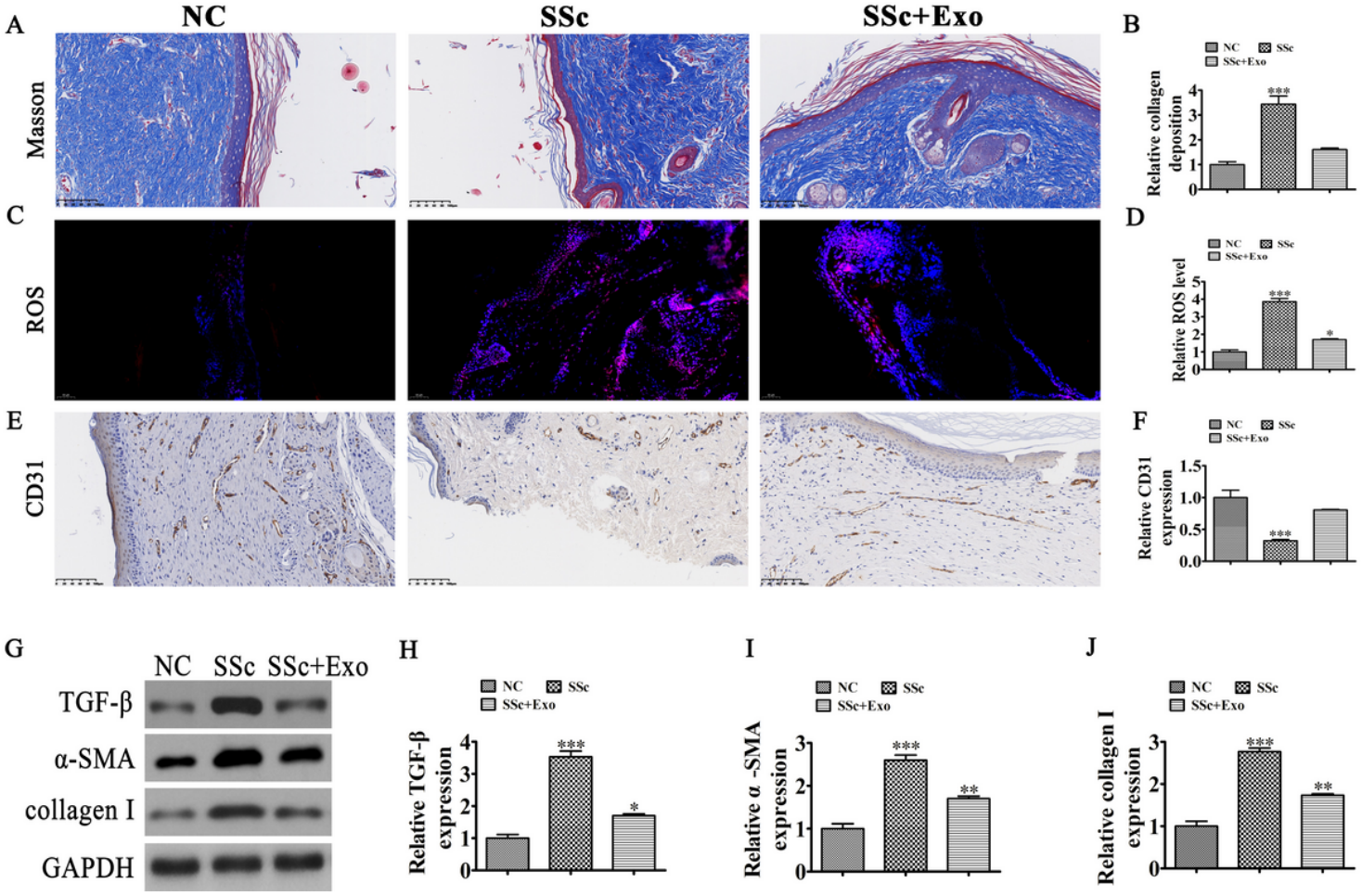

Figure 2

Masson's trichrome staining results in bleomycin-induced murine fibrosis model showed that collagen deposition was increased in bleomycin-induced scleroderma, while ADSC exosome treatment significantly decreased collagen deposition (A and B). Immunofluorescence detection of ROS staining validated that ADSC exosome treatment decremented ROS accumulation significantly in bleomycin-induced scleroderma (C and D). Immunohistochemical CD31 staining showed that angiogenesis was decreased in bleomycin-induced scleroderma. ADSC exosome treatment significantly reversed the inhibitory effect of scleroderma on angiogenesis (E and F). WB for fibroblast-associated proteins TGF-β, collagen I, and α-SMA showed that ADSC exosome treatment significantly decreased collagen I, α-SMA, and TGF-β expression in bleomycin-induced scleroderma (G–J).

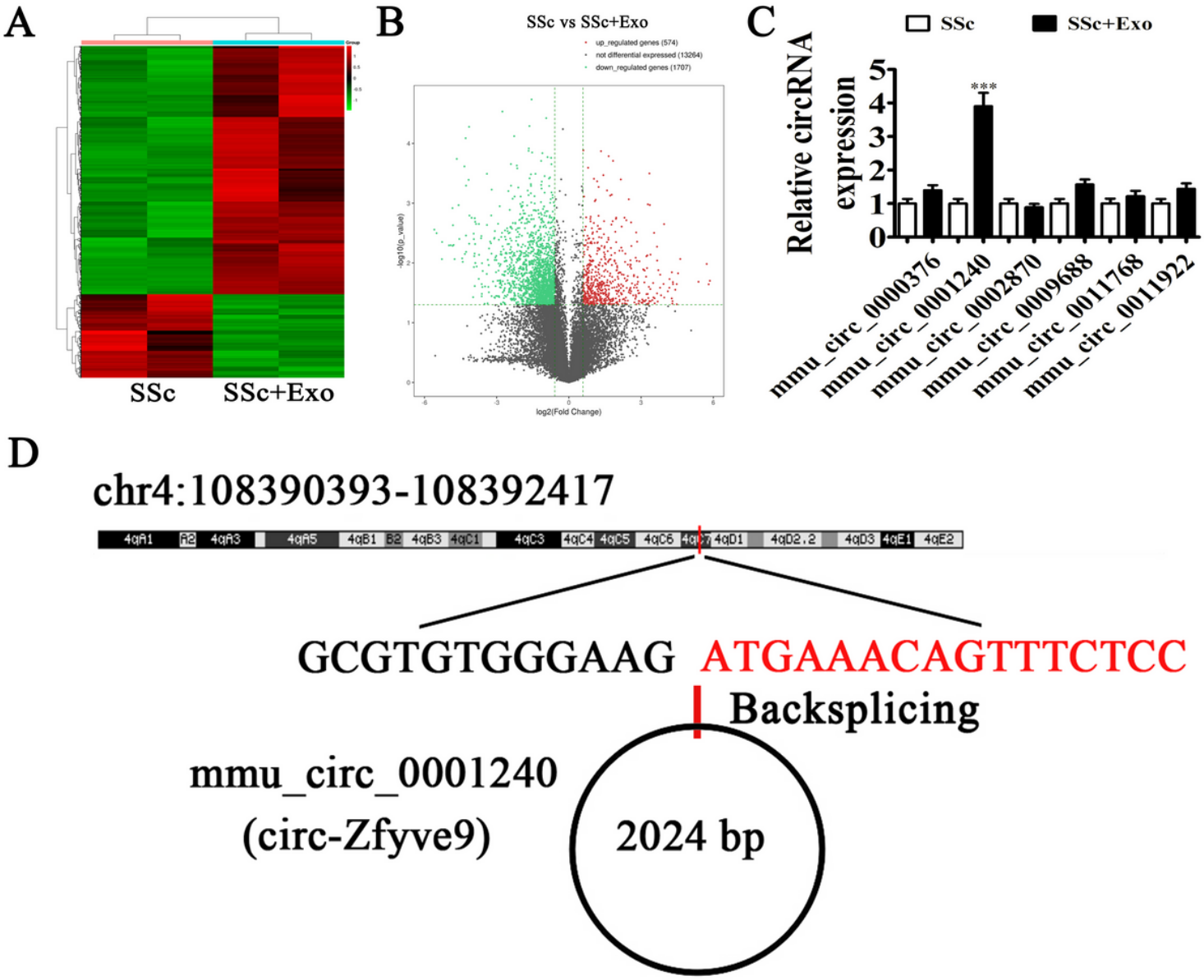

Figure 3

Heatmap analysis demonstrated that ADSC exosome treatment resulted in different circRNA expression levels (A). A total of 574 upregulated and 1707 downregulated circRNAs were found in ADSC exosome-treated scleroderma skin when compared to scleroderma skin without treatment (B). RT-qPCR showed that seven circRNAs from the sequencing analyses were upregulated, including mmu_circ_0000376, mmu_circ_0001240, mmu_circ_0002870, mmu_circ_0009688, mmu_circ_0011768, and mmu_circ_0011922. Data illustrated that only the mmu_circ_0001240 expression was upregulated in ADSC exosome-treated scleroderma skin when compared to scleroderma skin without treatment (C). Bioinformatics analysis found that mmu_circ_0001240 originated from the Zfyve9 gene exon (2024 bp) and was located in chr4:108390393-108392417. The mmu_circ_0001240 was named circ-Zfyve9 (D).

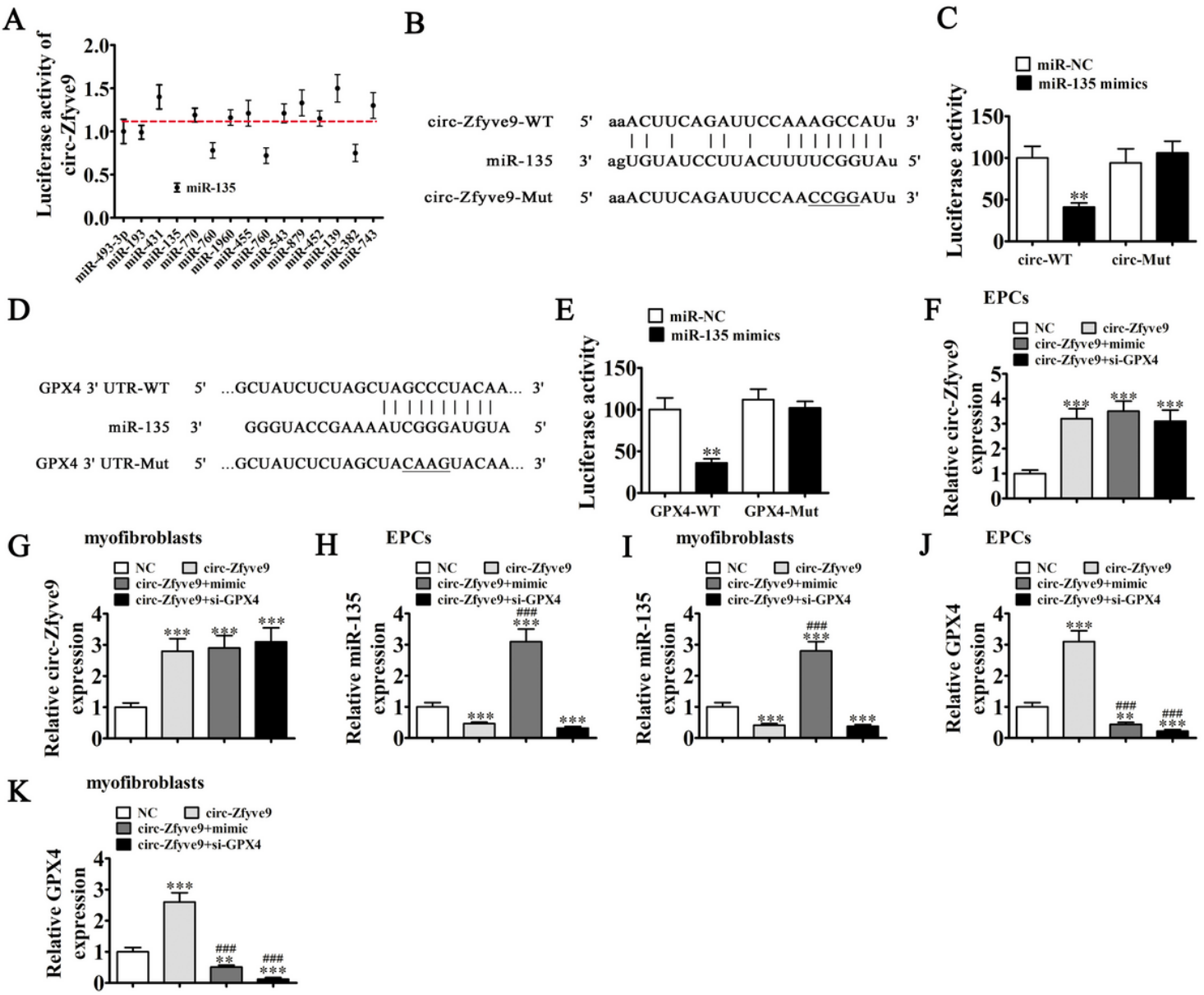

Figure 4

The results showed that miR-135 can decreament significantly fluorescein intensity, suggesting that miR-135 is circ-Zfyve9 downstream target (A). Luciferase reporter analysis verified that miR-135 inhibited luciferase activity in wild-type (WT), but not in mutated (MUT) cell lines (B and C), saying that miR-135 is a circ-Zfyve9 target. Bioinformatics results demonstrated that GPX4 is miR-135 downstream target. To further show a correlation between GPX4 and miR-135, we incorporated WT or MUT 3'UTR-GPX4 sequences including an miR-135 binding sequence into luciferase reporter vector (D). Our team transfected luciferase reporter vector into HEK293 cells, with or not miR-135 mimic. Luciferase reporter analysis showed that miR-135 inhibited luciferase function in WT, yet not in MUT cell lines (E), verifying that GPX4 is an miR-135 target. RT-qPCR results illustrated that circ-Zfyve9 expression was enriched in both EPCs and myofibroblasts after transfection using circ-Zfyve9 overexpression vector. Treatment with an miR-135 mimic or GPX4 silencing had no effect on circ-Zfyve9 expression in EPCs and myofibroblasts (F and G), suggesting that both miR-135 and GPX4 are located downstream of circ-Zfyve9. RT-qPCR

detection also found that circ-Zfyve9 overexpression decreased miR-135 expression. GPX4 silencing had no effect on circ-Zfyve9-induced miR-135 inhibition (H and I), suggesting that miR-135 is located between circ-Zfyve9 and GPX4. The results also found that circ-Zfyve9 overexpression increased GPX4 expression, while miR-135 upregulation reversed the promotion effect of circ-Zfyve9 on GPX4 expression. GPX4 expression decremented significantly after transfection with a GPX4 silencing vector (J and K), advising that circ-Zfyve9 enhanced GPX4 expression through sponging miR-135.

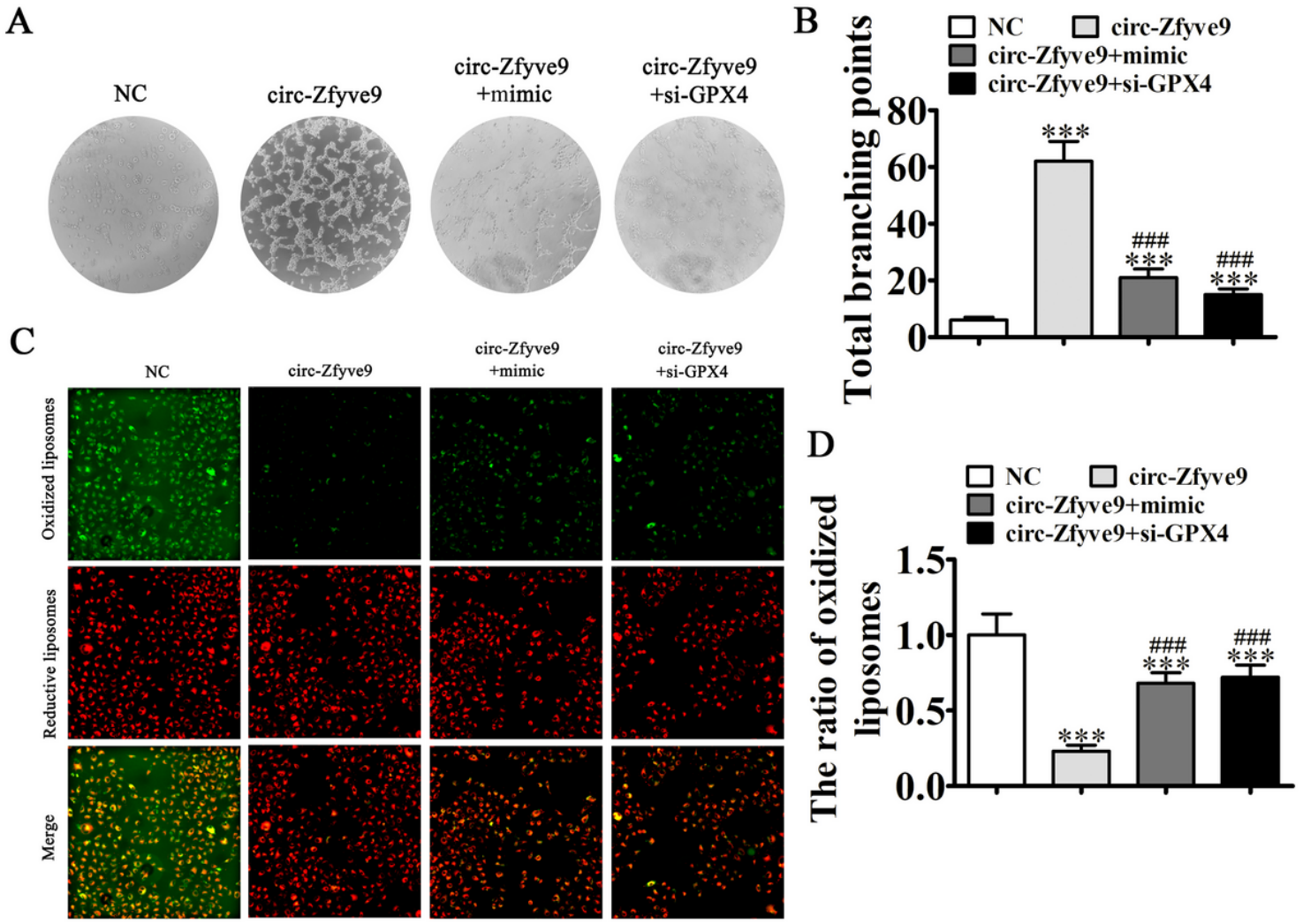

Figure 5

Overexpression of miR-135 or GPX4 silencing reversed the promotion of circ-Zfyve9 on the angiogenic differentiation of EPCs under hypoxic conditions (A and B), suggesting that miR-135 overexpression or GPX42 downregulation reversed circ-Zfyve9 promotion on angiopoiesis in EPCs under hypoxic conditions. Immunofluorescence detection showed that circ-Zfyve9 overexpression decreased liposomal oxidative stress by decreasing oxidized liposomes. Overexpression of miR-135 or GPX4 silencing reversed inhibitory circ-Zfyve9 effect upon hypoxia-induced liposome oxidative stress (C and D).

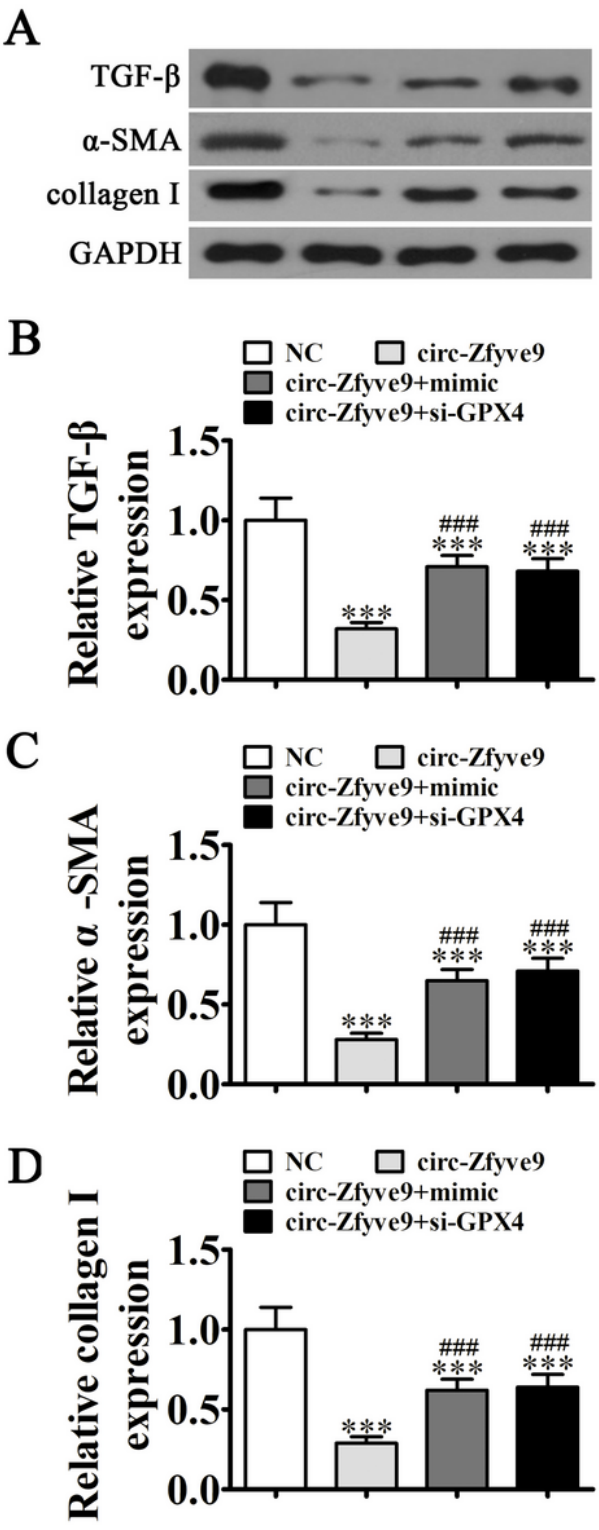

Figure 6

WB detection showed that circ-Zfyve9 overexpression decreased fibroblast-associated protein TGF-β, collagen I, and α-SMA expression in myofibroblasts under hypoxic conditions. Overexpression of miR-135 or GPX4 silencing reversed circ-Zfyve9 inhibitory effect upon hypoxia-induced fibroblast-associated protein TGF-β, collagen I, and α-SMA expression (A–D).

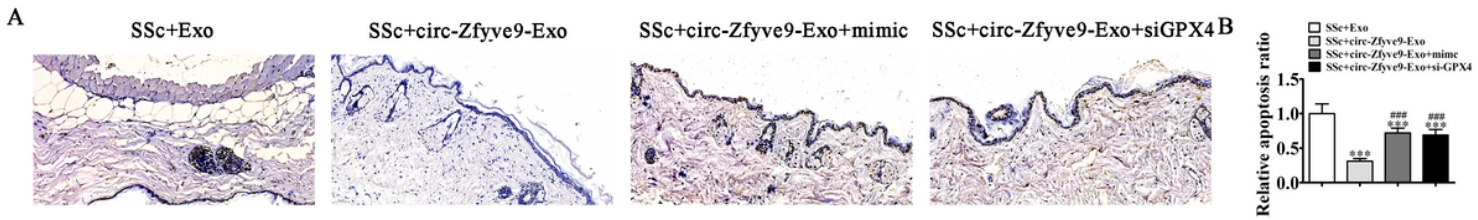

Figure 7

Immunohistochemical detection of apoptotic skin tissues showed the ADSC exosomes after treatment with overexpressed circ-Zfyve9. Apoptosis in skin tissues of bleomycin-induced scleroderma was decreased when compared to the ADSC exosome treatment group. Overexpression of miR-135 or GPX4 silencing reversed the protective effect of circ-Zfyve9 exosomes on apoptosis inhibition in bleomycin-induced scleroderma skin A and B), suggesting that circ-Zfyve9 overexpression increased the therapeutic effect of ADSC exosomes.